



A Discrete Element Method to simulate the mechanical behavior of ellipsoidal particles for a fusion breeding blanket



M. Moscardini ^{a,*}, Y. Gan ^b, R.K. Annabattula ^c, M. Kamlah ^a

^a Institute for Applied Materials, Karlsruhe Institute of Technology (KIT), Germany

^b School of Civil Engineering, The University of Sydney, Sydney, NSW, 2006, Australia

^c Department of Mechanical Engineering, Indian Institute of Technology Madras, Chennai, 600036, India

HIGHLIGHTS

- The influence of the particle shape on the bulk mechanical behavior of ceramic breeder was investigated.
- A DEM code was extended to analyse assemblies of ellipsoidal particles.
- A remarkable influence of the particles shape on the mechanical behavior of pebble beds was observed.
- A more compliant behavior was found in assemblies of particles with higher aspect ratios.

ARTICLE INFO

Article history:

Received 12 January 2017

Received in revised form 19 May 2017

Accepted 23 May 2017

Keywords:

Discrete element method

Pebble bed thermomechanics

Nuclear fusion

Multi-sphere approach

Ellipsoidal particles

ABSTRACT

The breeder materials proposed for the solid tritium breeding blanket concepts are ceramic lithium-based compounds in the form of pebble beds. Different fabrication processes have been developed to produce pebbles with a high sphericity. However, a small deviation from a perfectly spherical shape exists. In this paper the influence of non-sphericity on the mechanical behaviour of a pebble bed is assessed representing the currently produced pebbles by means of ellipsoidal particles. To this end, the in-house Discrete Element Method code KIT-DEM was further extended. The multi-sphere approach was implemented to generate the ellipsoidal particles while the existing random close packing algorithm was modified to create the assemblies. Uniaxial compression of the assemblies, under periodic boundary conditions, was simulated to investigate the bulk stress-strain behaviour of the bed. Sensitivity studies were carried out with different packing factors of the assembly and several aspect ratios of the particles. In agreement with previous studies carried on assemblies of spherical pebbles, the initial packing factor was found to noticeably affect the mechanical response of the investigated assemblies. Moreover, a remarkable influence of the shape on the mechanical behavior of the simulated assemblies was observed. Therefore it is concluded that for production techniques that result in poor sphericity, DEM simulations with non-spherical particles are necessary to reproduce realistic stress-strain behavior of pebble beds.

© 2017 Elsevier B.V. All rights reserved.

1. Introduction

The solid Breeding Blanket (BB) concepts make use of lithium-based ceramic pebble beds as tritium breeder. The pebbles are currently produced by different fabrication processes proposed by five members of the International Thermonuclear Experimental Reactor (ITER) agreement. The particles are characterized by a spheroidal shape with a maximum size around 1 mm to minimize volumetric swelling, thermal cracking as well as to ensure a homo-

geneous filling of the blanket [1–3]. The sphericity of the pebbles strongly depends on the fabrication method. Among the proposed processes both the sol-gel [4] and the melt-spraying [5] method show a high sphericity of 1.03 and 1.05, respectively.

The overall properties of pebble beds and their mechanical response depend strongly on the particle shape [6] as well as on the packing state [7,8]. A non-spherical particle shape could influence the bed response to external loads generating different stress levels, residual strains and micro response at the particle-scale compared to pebbles of a perfectly spherical shape. Moreover, the packing behavior as well as the packing structure could be affected by the particle shape, which in turn will further influence the mechanical response. All this, with regard to the breeder beds could have

* Corresponding author.

E-mail address: marigrazia.moscardini@kit.edu (M. Moscardini).

an impact on the configuration of the particles and the achievable packing factor, as well as on the occurrence of ratcheting, pebble breakage and gap formation between pebble bed and container wall. Consequently, understanding the effects of pebble shape is of significance with respect to pebble production and breeder zone design.

To model non-spherical particles, several numerical methods were proposed in the community of the Discrete Element Method (DEM). A brief overview of four main approaches is reported in the following: (1) The super quadratic method describes the shape of non-spherical particles mathematically. In particular one choice (1-a) is to discretize the surface of the particle by individual points meaning that a uniform discretization by equally spaced points is suitable for perfectly symmetrical particles while an adaptive discretization is used to represent particles with sharp vertices or edges for whom a large amount of points are required [9]. Another option (1-b) is a representation by a continuous function. The main weakness of the continuous function method is the use of an elaborate contact algorithm while the drawback of the particle surface discretization is the high computational time. (2) The polygons/polyhedrons methods allow generating shapes with sharp edges or flat surfaces. It has a very high stability however a very complex contact detection algorithm is needed [6]. (3) The Multi-Sphere (MS) method is a very robust approach and it was selected to represent the ellipsoidal particles in this work. It relies on representing different shapes by several overlapping primary spheres, such that the outer surface of the compound of the primary spheres represents the particle shape [6,10,11]. The main advantage of the MS method is that the robust contact algorithm developed for spherical particles is still applicable between the primary spheres of two non-spherical particles in contact. However, the computational time increases with the number of the primary spheres required to reach the desired level of smoothness of the particle surface. Furthermore, owing to the intrinsically non-convex surface of the particles, multiple contacts could occur overestimating the resulting contact forces. Höhner proposes in [12] a method to reduce the effect generated by Multi Contacts (MCs), introducing a “correction” by dividing, at each time step, the increment of the normal and tangential force by the number of the contact points between two particles.

Starting from the in-house code KIT-DEM [7], several modifications have been implemented to generate assemblies of ellipsoidal particles in order to study their mechanical behavior. In the next section the algorithm implemented to create the assemblies of ellipsoidal particles is described. Section 3 explains in detail the DEM code used to simulate the compression of the assemblies. The numerical results are reported in Section 4 while the conclusions are drawn in Section 5.

2. Generation of assemblies of ellipsoidal particles

This section presents the developed algorithm to generate assemblies consisting of composite ellipsoidal particles. It consists of two subsections. The first subsection provides a detailed overview of the MS method while in the second subsection the modifications of the existing Random Close Packing (RCP) algorithm are described.

2.1. Multi-sphere approach

In the MS approach several primary spheres in overlap are clustered to form approximately the desired geometry. The size, the number and the overlap of the primary spheres can be tailored to obtain the desired shape. To maintain the geometry the relative position between the primary spheres of a single particle must

not change. For an ellipsoidal shape an odd number of primary spheres is suggested to simplify the implementation of the equations of motion. The studies reported in this paper were performed on assemblies consisting of mono-sized ellipsoidal particles. The implementation of the MS method in this code was limited to clustering three mono-sized spheres to create each ellipsoidal particle. This limitation was sufficient to represent the pebbles currently produced and, more important, developing an understanding of some basic effects of non-spherical particles. The number of the particles in a bed and the aspect ratio are set as input parameters. The aspect ratio a_r is defined as the ratio between the major axis of the ellipsoidal particle generated and the diameter of the primary spheres. Furthermore, the overlap (δ_s) is related to the aspect ratio, to the number of the clustered primary spheres (N_s) and to their radius (R) as

$$\delta_s = \delta R, \quad (1)$$

where

$$\delta = 2 \frac{N_s - a_r}{N_s - 1} \quad (2)$$

is the fraction of the radius in overlap.

Initially all spheres required to create the ellipsoidal particles are randomly generated in a cubic box with an edge length L (Fig. 1a). In this work 15,000 spheres are generated to create 5000 ellipsoidal particles. Each ellipsoidal particle and each sphere is numbered sequentially. According to the assigned number the spheres are then classified in three groups, namely spheres “a” (from 1 to 5000), spheres “b” (from 5001 to 10,000) and spheres “c” (from 10,001 to 15,000). Each ellipsoidal particle is formed by aligning three spheres belonging to the groups “a”, “b” and “c” with a fixed distance and overlap depending on the desired aspect ratio. The spheres “a” and “b” become the external primary spheres of the ellipsoidal particle while the sphere “c” is placed in the middle of the line joining centers of “a” and “b” to complete the formation of an ellipsoidal particle (Fig. 1b). In particular the ellipsoidal particle number 1 is created moving the sphere “b” 5001 in the direction of the sphere “a” 1, thereafter the sphere “c” 10,001 is moved in the middle (Fig. 1a). With the same method the other ellipsoidal particles are generated (e.g., the ellipsoidal particle number i is composed by the spheres i , $5000 + i$ and $10,000 + i$ belonging to the groups “a”, “b” and “c”, respectively). The coordinates of the motion of a sphere “b” along the line showed in Fig. 1a are given by:

$$\begin{cases} x(t_f) = x_a + t_f(x_b - x_a) \\ y(t_f) = y_a + t_f(y_b - y_a) \\ z(t_f) = z_a + t_f(z_b - z_a) \end{cases}, \quad (3)$$

where subscript a indicates the position of sphere “a”, while subscript b indicates the initial position of sphere “b”. The value t_f for the final position $(x(t_f), y(t_f), z(t_f))$ of sphere “b” is chosen such that a given aspect ratio a_r is obtained. For the composite particle, the aspect ratio is given by:

$$a_r = \frac{d + 2R}{2R}, \quad (4)$$

where R is the radius of a primary sphere and

$$d = \sqrt{(x(t_f) - x_a)^2 + (y(t_f) - y_a)^2 + (z(t_f) - z_a)^2}, \quad (5)$$

is the distance between the two external spheres in the final configuration. Plugging $x(t_f)$, $y(t_f)$, $z(t_f)$ into Eq. (5) and defining the

value of d in function of the aspect ratio from the Eq. (4) the value of t_f is obtained as

$$t_f = \frac{d}{\sqrt{(x_b - x_a)^2 + (y_b - y_a)^2 + (z_b - z_a)^2}} \quad (6)$$

The final position of the center of sphere b is obtained from inserting the solution t_f into Eq. (3).

When all particles are formed two different kinds of overlaps exist. The first (δ_s as given in Eq. (1)) is between the primary spheres composing the same ellipsoidal particle (Fig. 1b) while the second (δ_p) occurs between the spheres of two different ellipsoidal particles in contact (Fig. 2a). This is an artifact due to placing primary spheres randomly and forming composite particles from them. The next subsection deals with the procedure to remove this second kind of unphysical overlaps from the assembly.

2.2. Random Close Packing Algorithm

The Random Close Packing Algorithm (RCP), first proposed by Jodrey and Tory [13] and successively used by Gan et al. [7,14] to generate random and densely packed assemblies of spherical particles, was adapted in order to be consistent with the MS method previously described. The modified RCP iteratively eliminates the overlap δ_p between two ellipsoidal particles in contact (Fig. 2a). The primary spheres are characterized by an outer radius R_{out} and inner radius R_{in} as schematically shown in Fig. 2b. These two values are the same for all primary spheres and they are defined as follows: R_{out} characterizes overlaps between particles. On the contrary the inner radius R_{in} , defined as the half of the distance between the centers of the two closest primary spheres of two different ellipsoidal particles, is the value for which no overlap between ellipsoidal particles occurs in the whole assembly. These two radii are adjusted to approach each other step by step by removing the worst overlap of the current iteration. When $(R_{out} - R_{in})/R_{out}$ falls below a certain threshold, the assembly is considered to be free of overlaps and the final configuration is reached.

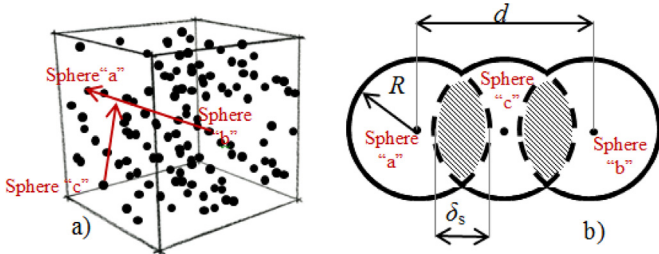


Fig. 1. a) Centers of the spheres in the virtual cubic box; b) Composed ellipsoidal particle.

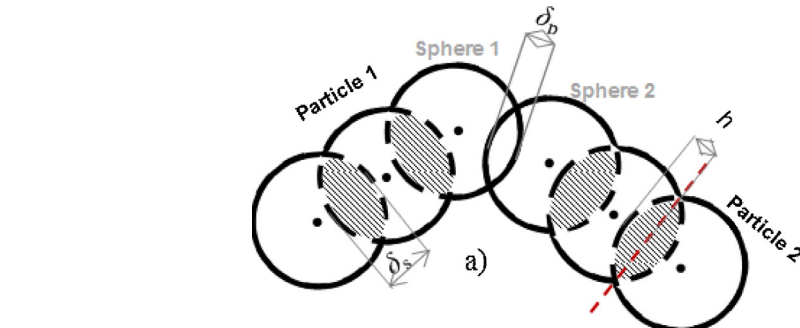


Fig. 2. a) Ellipsoidal particles in overlap; b) Outer and inner radius of spheres.

The details related to the generation of the starting configuration and to the iteration process are described below. The initial configuration is defined as follows. First, the spherical particles are generated randomly into the virtual cubic box (Fig. 1a) as described in the previous subsection. Afterwards, the initial value of R_{out} is set to get an ideal starting packing factor ($PF^{(0)}$) equal to 1 [13]. The PF_i is expressed as the ratio between the volume taken by the ellipsoidal particles and the volume of the box as

$$PF^{(0)} = \frac{V_p N_p}{V} = 1, \quad (7)$$

where V_p and N_p are the volume and the number of the composed ellipsoidal particle contained in the volume V of the virtual box, respectively. Implementing the volume of the ellipsoidal particles, the volume in overlap introduced by the union of the primary spheres is subtracted. Therefore the volume of the composed ellipsoidal particle is calculated as difference between the volume of the three primary spheres and the volume of the spherical caps in overlap as

$$V_p = (V_s N_s - V_{sc} 2(N_s - 1)), \quad (8)$$

where N_s is the number of the primary spheres clustered to form the ellipsoidal particle and $(N_s + 1)$ is the number of the spherical caps in overlap. The volume of one spherical cap V_{sc} and the volume of one sphere are given by

$$V_{sc} = \pi h^2 \left(R_{out} - \frac{h}{3} \right); V_s = \frac{4}{3} \pi R_{out}^3, \quad (9)$$

where h , as shown in Fig. 2a, is the height of the spherical cap. Besides h is also half of the distance in overlap and it is evaluated as

$$h = \frac{R_{out} \delta}{2}. \quad (10)$$

Plugging h into Eq. (9) and then V_{sc} into the Eq. (8) the volume of the composed ellipsoidal particles is defined as a function of R_{out} . Substituting V_p into the Eq. (7) R_{out} is defined as a function of $PF^{(0)}$. Finally, the ellipsoidal particles are created considering R_{out} as the starting radius by means of the MS method described in the previous subsection. Now the initial configuration is ready and the iteration process is started. The initial value of R_{out} defines the largest overlap between any two particles in the assembly and it is the largest value assumed by R_{out} during the entire simulation. On the other hand, due to its definition, the initial value of R_{in} is the smallest value evaluated during the entire simulation.

During each iteration the code detects the overlaps between primary spheres of contacting particles and creates a list starting from the largest overlap. The inner radius is then calculated as function of the worst overlap as defined above and the primary spheres in contact are moved away from each other equally by a distance of $R_{out} - R_{in}$ along the line that connects the two centers. Then the

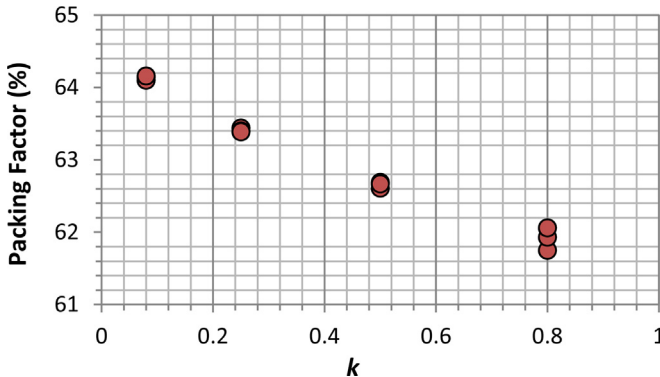


Fig. 3. Packing factor obtained from selected values of contraction rate k for assemblies of 5000 ellipsoidal particles with an aspect ratio of ~ 1.12 .

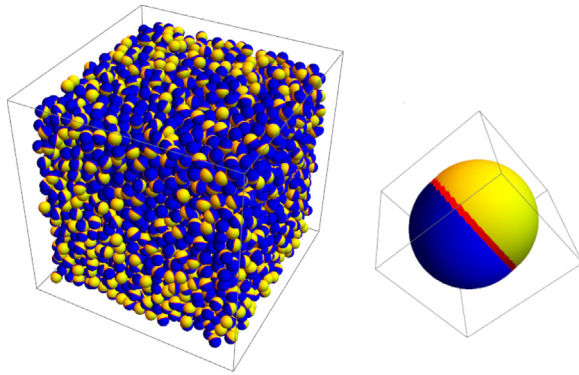


Fig. 4. Assembly of 5000 mono-sized ellipsoidal particles composed of 3 equal-sized spheres in overlap.

other primary spheres composing the ellipsoidal particles in contact are accordingly moved to maintain the particle's shape and spatial orientation.

Afterwards, as described in Ref. [14] the outer radius is contracted according to

$$\chi^{i+1} = \chi^i \frac{(1/2)^j k}{N_p}, \quad (11)$$

where $\chi^i = R_{\text{out}}^{(i)}/R_{\text{out}}^{(0)}$ and $j = [-\log_{10} \Delta \eta^{(i)}]$. Here, i is the iteration number, and $\Delta \eta$ is the difference between the packing factors calculated by R_{out} and R_{in} . More details are reported in Ref. [15] for random packing of spherical particles. The parameter k is the contraction rate, and it is the input parameter that controls how fast the outer radius is contracted in each iteration step. As reported in Ref. [15], the resulting packing factor can be roughly controlled by k . In order to check this relation for ellipsoidal particles, we generated three assemblies for each value of k . The assemblies consisted of 5000 ellipsoidal particles with an aspect ratio of ~ 1.12 , each particle being composed of 3 primary spheres. In Fig. 3 the obtained packing factors for the selected values of k are reported.

First, we observe that for the same value of contraction rate nearly the same packing factor is obtained for different assemblies. Second, the trend of an increase of the packing factor with decreasing contraction rate can clearly be recognized. This together confirms that also for the ellipsoidal particles considered here the packing factor of an assembly can roughly be controlled by the contraction rate.

Thus, it was shown how the random close packing algorithm as introduced for spheres in [7,13–15] was adapted to generate assemblies composed by ellipsoidal particles.

The assemblies are visualized with Mathematica 10.3 [16]. Fig. 4 exemplarily shows one of the generated assemblies of ellipsoidal particles having an aspect ratio of ~ 1.12 and an overlap between the primary spheres of $\sim 1.88R$.

3. Discrete element method for ellipsoidal particles

DEM is a powerful computational tool to investigate the micromechanics of granular materials. Particles composing the assembly are individually identified with their shape, mass, physical and mechanical properties. The behavior of the assembly is modelled by detecting the contact interactions between particles and then by tracking the motion of each particle. Each interaction is defined by the implemented contact model while the particles' motion is described by the Newton and the Euler differential equations of motion. The macroscopic behavior of the assembly is then obtained from the computed motion of each particle composing the assembly.

3.1. Mechanical interaction

In this work, numerical simulations for assemblies of ellipsoidal particles have been carried out. Uniaxial compression tests (UCT) are simulated by applying a prescribed deformation to the assembly of particles in a series of load steps separated by time increments Δt . After each change of the prescribed deformation, the equations of motion are solved until an equilibrium state is reached. Artificial damping [7] is introduced to gradually remove all kinetic energy from the system to reach the quasi-static condition. During such a physical process of relaxation towards equilibrium, the equations of motion are solved numerically by an explicit time stepping scheme.

As previously described, the ellipsoidal particles were generated by means of the MS method and the contact detection was carried out between the primary spheres composing different particles. Therefore, the contact detection algorithm developed for spherical particles in Ref. [7], is still applicable. The contacts are considered to be purely elastic with normal and tangential interactions. The normal force is evaluated by the Hertzian contact law [17]

$$\mathbf{f}_{N,j}^{(I_n, Q_m)} = -\frac{4}{3}E * \sqrt{R_*} (\delta_j)^{3/2} \mathbf{n}_j. \quad (12)$$

Here, $\mathbf{f}_{N,j}^{(I_n, Q_m)}$ is the normal force between the two primary spheres n and m constituting the different particles I and Q in contact j . Here the subscripts m and n represent the primary sphere a , b or c , as explained in Section 2. Furthermore, δ_j is the overlap in contact j between the two primary spheres constituting the two different particles I and Q , while \mathbf{n}_j is the outward normal at the primary sphere in contact j . Finally, since the particles in contact are made of the same material in our case, the effective Young's modulus E^* is expressed as $E^* = E/2 (1 - \nu^2)$, while the reduced radius R^* is defined as $R^* = R/2$ for the present case of mono-sized particles.

The tangential force acting between I_n and Q_m is taken as the minimum between the friction and the shear force according to Ref. [18] as

$$\mathbf{f}_{T,j}^{(I_n, Q_m)} = -\frac{\Delta \dot{\mathbf{x}}_{T,j}}{|\Delta \dot{\mathbf{x}}_{T,j}|} \min(\mu |\mathbf{f}_{N,j}^{(I_n, Q_m)}|; k_s R_a |\Delta \dot{\mathbf{x}}_{T,j}| \Delta t), \quad (13)$$

where $\Delta \dot{\mathbf{x}}_{T,j}$ is the sliding velocity in contact j that occurs between the two primary spheres constituting different particles, i.e. the difference in velocities of the surfaces of the corresponding primary spheres in this contact. Furthermore, the parameters μ and k_s are the friction coefficient of the contacting surfaces and the shear stiffness, respectively. Last, R_a is the radius of the contact area, which

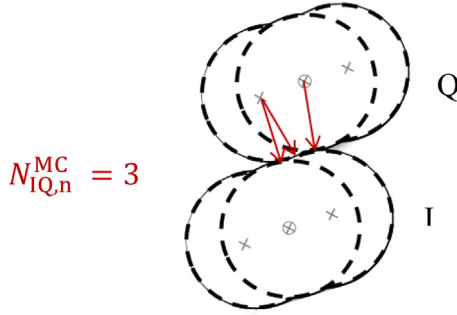


Fig. 5. Multiple contacts between two particles I and Q at some time step n.

is expressed as $R_a = \sqrt{\left(\frac{1}{R_{Qm}} + \frac{1}{R_{In}}\right)\delta_p}$ [17]. The contact forces acting on I_n are applied to Q_m with the same magnitude but opposite orientation to satisfy the principle of action and reaction. As shown in Fig. 5, due to the shape approximation introduced by the MS method, more than one contact can occur between two particles.

This phenomenon is called multi-contact (MC). This means that the code can detect more than one contact acting on the particle I from the same primary sphere of the particle Q. The number of the multi-contacts N_{IQ}^{MC} between two particles I and Q depends on the number of the primary spheres, on the overlap between them and on the relative position of the two contacting particles. In particular, for two particles in contact each being composed of three primary spheres, the maximum number of multiple contacts is 9. The possibility of multiple contacts (Fig. 5) is an intrinsic feature of the MS geometry, which does not happen between true ellipsoids due to their convexity. However, since we want to approximate real ellipsoids by MS particles, we need to deal with artifacts due to multiple contacts such as overestimation of the resulting stresses.

To approach the ellipsoid situation by reducing the effect of the multiple contacts, it was suggested in Ref. [12] to divide the increment of both normal and tangential force at each time step n by the current number $N_{IQ,n}^{MC}$ of multiple contacts between particles I and Q. Thus, the contact forces are updated based on the previous value of time step n – 1. The normal force is updated according to

$$\hat{f}_{N,kq,n}^{(I,Q)} = \hat{f}_{N,kq,n-1}^{(I,Q)} + \frac{\Delta f_{N,kq,n}^{(I,Q)}}{N_{IQ,n}^{MC}}; \quad k_q = 1, \dots, N_{IQ,n}^{MC}, \quad (14)$$

where $\hat{f}_{N,kq,n}^{(I,Q)}$ represents the adjusted magnitude of the normal force at time step n in a multiple contact k_q , which particle I has with particle Q. Furthermore, the increment $\Delta f_{N,kq,n}^{(I,Q)}$ is the difference between $f_{N,kq,n}^{(I,Q)}$ and $f_{N,kq,n-1}^{(I,Q)}$, which are the corresponding magnitudes of Eq. (12) at time steps n and n – 1, respectively.

The procedure to scale the tangential force on the multi contacts number requires a further observation. At each time step the magnitude of the tangential force is defined as the minimum value between the friction force and the shear force, as reported in Eq. (13). At this point the magnitude of the friction force, which depends on the normal force, is already updated by means of Eq. (14). Therefore to avoid a further adjustment of the friction force during the same iteration the code scales only the magnitude of the shear force according to

$$\hat{f}_{T_s,kq,n}^{(I,Q)} = \hat{f}_{T_s,kq,n-1}^{(I,Q)} + \frac{\Delta f_{T_s,kq,n}^{(I,Q)}}{N_{IQ,n}^{MC}}; \quad k_q = 1, \dots, N_{IQ,n}^{MC}. \quad (15)$$

In Eq. (15), $\hat{f}_{T_s,kq,n}^{(I,Q)}$ represents the adjusted magnitude of the shear force at time step n in a multiple contact k_q , which particle I

has with particle Q. $\Delta f_{T_s,kq,n}^{(I,Q)}$ is the difference between $f_{T_s,kq,n}^{(I,Q)}$ and $f_{T_s,kq,n-1}^{(I,Q)}$, which are the magnitudes of the shear force $k_s R_a |\Delta \dot{x}_{T,j}| \Delta t$ at time steps n and n – 1 respectively. Afterwards the minimum value between the friction and the shear force is evaluated. The adjusted magnitude of the normal force from Eq. (14) is then multiplied by the normal unit vector giving

$$\hat{f}_{N,j}^{(I_n,Q_m)} = \hat{f}_{N,kq,n}^{(I,Q)} \mathbf{n}_j \quad (16)$$

On the other hand, the adjusted magnitude of the tangential force, which is the minimum value between $\mu \hat{f}_{N,kq,n}^{(I,Q)}$ and $\hat{f}_{T_s,kq,n}^{(I,Q)}$, is multiplied by the tangential unit vector yielding.

$$\hat{f}_{T,j}^{(I_n,Q_m)} = -\frac{\Delta \dot{x}_{T,j}}{|\Delta \dot{x}_{T,j}|} \min(\mu \hat{f}_{N,kq,n}^{(I,Q)}, \hat{f}_{T_s,kq,n}^{(I,Q)}), \quad (17)$$

The principle of action and reaction is satisfied, as the same adjusted contact force magnitudes are taken to act on particle Q. Details related to this approach are reported in Ref. [12]. Once the normal force $\hat{f}_{N,j}^{(I_n,Q_m)}$ and tangential force $\hat{f}_{T,j}^{(I_n,Q_m)}$ are determined for each contact j between I_n and Q_m , their vectorial sum is used to evaluate the total force.

$$\mathbf{F}_{TOT}^I = \sum_j (\hat{f}_{N,j}^{(I_n,Q_m)} + \hat{f}_{T,j}^{(I_n,Q_m)}) \quad (18)$$

acting on the particle I, as well as the external torque.

$$\mathbf{M}_{TOT}^I = \sum_j \mathbf{r}_j \times (\hat{f}_{N,j}^{(I_n,Q_m)} + \hat{f}_{T,j}^{(I_n,Q_m)}) \quad (19)$$

where \mathbf{r}_j is the position vector between the contact point j and the center of mass of the ellipsoid. The resulting forces \mathbf{F}_{TOT}^I evaluated as the vectorial sum of the all forces acting on the three primary spheres clustered to form the ellipsoidal particle and the torques \mathbf{M}_{TOT}^I acting on the particles determine their motion in the assembly. In classical mechanics the motion of a rigid body is described by a translational and a rotational motion. The translational motion is independent of the particle shape and it is defined by means of Newton's second law

$$m^I \ddot{\mathbf{x}}^I = \mathbf{F}_{TOT}^I \quad (20)$$

where m^I and $\ddot{\mathbf{x}}^I$ are the mass and the position vector of the center of mass of particle I, respectively.

3.2. Equations of motion

Unlike the translational motion the rotation is affected by the particle shape. For a non-spherical particle the implementation of the moment of inertia in the global coordinate system is cumbersome. In order to simplify the implementation of the tensor of the moment of inertia, the rotational motion is expressed in a local coordinate system instead of the global coordinate system fixed to the assembly's cubic box. The origin of the local coordinate system is located at the center of mass of the particle with the axes oriented along the main axes of inertia as shown in Fig. 6. Due to the particle's symmetry, the inertia tensor becomes in this coordinate system diagonal containing only the principal moments of inertia of a real ellipsoid I_{xx} , I_{yy} and I_{zz} .

The rotational accelerations in the local frame are then evaluated by means of the Euler equations [19]

$$\begin{aligned} M_{x,L}^I &= \dot{\omega}_{x,L}^I I_{xx} + (I_{zz} - I_{yy}) \omega_{y,L}^I \omega_{z,L}^I \\ M_{y,L}^I &= \dot{\omega}_{y,L}^I I_{yy} + (I_{xx} - I_{zz}) \omega_{x,L}^I \omega_{z,L}^I, \\ M_{z,L}^I &= \dot{\omega}_{z,L}^I I_{zz} + (I_{yy} - I_{xx}) \omega_{y,L}^I \omega_{x,L}^I \end{aligned} \quad (21)$$

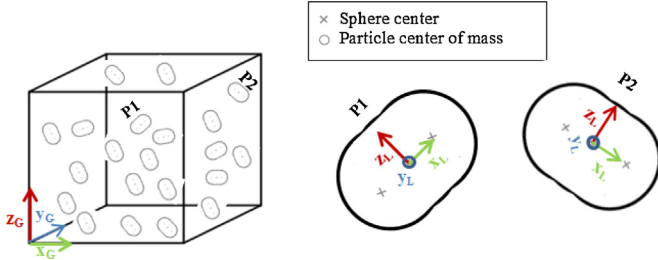


Fig. 6. Global and local coordinate system.

where $\omega_{x,L}^l$, $\omega_{y,L}^l$, and $\omega_{z,L}^l$ are the components of the vector ω_L^l of angular velocity in the local coordinate system L, while $M_{x,L}^l$, $M_{y,L}^l$, and $M_{z,L}^l$ are the components of the vector of the resulting torque \mathbf{M}_{TOT}^l acting on particle I in the local coordinate system. Eq. (21) can be solved for the vector of rotational acceleration, which can then be transformed into the global coordinate system G to calculate the velocities and the positions of the particles by means of the Verlet Algorithm for the integration of the ordinary differential equations of motion [20,21]. The transformations between the two coordinate systems are performed via a rotation matrix. The rotation matrix can be expressed in terms of Euler angles or in terms of quaternions. However, the first approach suffers from the gimbal lock singularity. Therefore, due to the absence of singularities, the unit quaternion approach is used in this work for the coordinate transformation. In the next subsection the unit quaternion method and its implementation in the code is described.

3.3. The unit quaternions method for the rotational motion

Quaternions were introduced in the nineteenth century by Hamilton [22]. Quaternions were successively used to describe the rotational motion of a particle defining its orientation in space [23–25]. For the algebra of quaternions and their application to the 3D motion of non-spherical particles, we refer to Ref. [26] and the works cited there.

A quaternion

$$\mathbf{q} = q_0 \mathbf{q} \quad (22)$$

is composed of a scalar q_0 and a vector part

$$\mathbf{q} = q_1 \mathbf{i} + q_2 \mathbf{j} + q_3 \mathbf{k}. \quad (23)$$

Here, q_0 , q_1 , q_2 and q_3 are real numbers and \mathbf{i} , \mathbf{j} and \mathbf{k} are unit vectors along to the x , y and z axis, respectively. By means of so-called unit quaternions the pure rotation of a vector is described by two geometrical quantities: the angle of rotation α and the unit vector $\check{\mathbf{q}}$ about which the rotation takes place. Accordingly, such unit quaternion is defined as

$$\mathbf{q} = [\cos \frac{\alpha}{2}, \sin \frac{\alpha}{2} \check{\mathbf{q}}], \quad (24)$$

where

$$\|\check{\mathbf{q}}\| = 1. \quad (25)$$

As described in Section 3, after prescribing a load step, the numerical integration of the equations of motion during a relaxation process towards equilibrium is based on time steps. At time step n, by means of the angle of rotation

$$\alpha_n = \|\omega_n\| \Delta t \quad (26)$$

and the normalized vector

$$\check{\mathbf{q}}_n = \frac{\omega_n}{\|\omega_n\|} \quad (27)$$

about which the rotation takes place, the unit quaternion $\hat{\mathbf{q}}_n$ taking the particle from time step $n - 1$ to time step n is expressed as

$$\hat{\mathbf{q}}_n = [\cos \frac{\|\omega_n\| \Delta t}{2}, \sin \frac{\|\omega_n\| \Delta t}{2} \frac{\omega_n}{\|\omega_n\|}], \quad (28)$$

Here, ω_n is the angular velocity at time step n and Δt is the time increment between time steps, meaning that $\hat{\mathbf{q}}_n$ represents the variation of the orientation in a time step Δt . To represent the change from the initial orientation of a particle to the current orientation at time step n direct multiplication method was implemented. In this approach [26,27], the unit quaternion at the current time step n is evaluated by

$$q_{n-1} = \prod_{m=1}^{n-1} \hat{\mathbf{q}}_{n-m}, \quad (29)$$

$$q_n = \hat{\mathbf{q}}_{n-1} q_{n-1}, \quad (30)$$

where $\hat{\mathbf{q}}_{n-1}$ is the unit quaternion between the time steps $n - 2$ and $n - 1$, while q_{n-1} is the product of the unit quaternion between the time step $n - 1$ and $t=0$. Therefore q_{n-1} represents the total rotation from the original orientation at $t=0$ to the orientation at time step $n-1$. The non-commutative multiplication of quaternions is defined as $pq = [p_0 q_0 - \mathbf{p} \cdot \mathbf{q}, p_0 \mathbf{q} + q_0 \mathbf{p} + \mathbf{p} \times \mathbf{q}]$, which can also be represented by a matrix operation [26]. In this updating method the typical approach based on Taylor series is avoided and the multiplication replaces the addition operator in the integral equation. The multiplication between unit quaternions preserves their unit length and the further re-normalization, usually adopted after the addition operation, can be avoided. Once the components of quaternion q_n are defined in the global coordinate system, the rotation matrix

$$\underline{\underline{R}} = \begin{pmatrix} 1 - 2(q_2^2 + q_3^2) & 2q_1q_2 - 2q_0q_3 & 2q_0q_2 + 2q_1q_3 \\ 2q_1q_2 + 2q_0q_3 & 1 - 2(q_1^2 + q_3^2) & 2q_2q_3 + 2q_0q_1 \\ 2q_1q_3 - 2q_0q_2 & 2q_0q_1 + 2q_2q_3 & 1 - 2(q_1^2 + q_2^2) \end{pmatrix} \quad (31)$$

can be obtained. By means of the rotation matrix, the transformations between the global and the local coordinate systems L and G can be carried out as

$$\begin{matrix} V_{x,L} & V_{x,G} \\ (V_{y,L}) & = \underline{\underline{R}}(V_{y,G}), \\ V_{z,L} & V_{z,G} \end{matrix} \quad (32)$$

$$\begin{matrix} V_{x,G} & V_{x,L} \\ (V_{y,G}) & = \underline{\underline{R}}^T(V_{y,L}), \\ V_{z,G} & V_{z,L} \end{matrix} \quad (33)$$

Here, $\underline{\underline{R}}^T$ is the transposed rotation matrix, while the column matrices $\underline{\underline{V}}_L = (V_{x,L}, V_{y,L}, V_{z,L})^T$ and $\underline{\underline{V}}_G = (V_{x,G}, V_{y,G}, V_{z,G})^T$ consist of the Cartesian components of some vector \mathbf{V} in local and global coordinates, respectively.

In the present study the rotation matrix is used to transform the column matrix $\underline{\underline{M}}_{TOT,G}^l$ of the torque, Eq. (19) and the column matrix of the rotational velocity ω_G^l from the global to the local coordinate system through Eq. (32). Based on these local components, the components of the rotational acceleration in the local coordinate system are obtained from Eq. (21). Afterwards, the transposed rotation matrix is used to transform the column matrix $\dot{\omega}_L^l$ of the rotational accelerations from the local to the global coordinate system by means of Eq. (33). This has to be done for each ellipsoidal particle at each time step n. Furthermore, the quaternion and the rotation matrix of every particle need to be updated at each time step.

4. Numerical simulations and discussion

In this work, the existing in-house DEM code was extended in the way described above to simulate the uniaxial compression of assemblies consisting of ellipsoidal particles.

In order to represent the bulk behaviour of the pebble bed in the blanket, periodic boundary conditions were applied all around a virtual box consisting of packed ellipsoidal particles. Using periodic boundary conditions, any wall effect on the packing structure is avoided, while the bulk behaviour of the pebble bed in the blanket is reproduced with a reasonably low number of particles (5000 in this study). Periodic boundaries were already implemented for spheres in the existing KIT-DEM-code [7,15]. For ellipsoidal particles, the implementation was slightly modified to consider each ellipsoidal boundary pebble as a cluster of three spheres. Further details about the implementation of periodic boundary conditions for packed spheres are reported in [7].

The assemblies are gradually compressed applying a constant strain increment (1.25e-3% for simulations with ellipsoidal particles and 2.5e-3% for simulations with spheres) in one direction called the axial direction up to the maximum strain of 1.25%. The applied strain increments are chosen to represent quasi-static loading conditions. The maximum macroscopic axial strain of 1.25% is used in accordance with a previous study [7]. To represent the so-called uniaxial compression test (UCT), the assembly is kept at fixed width in the other two space dimensions perpendicular to the direction of uniaxial loading, while the periodicity of the system is maintained.

When the maximum strain is reached, the assembly is gradually unloaded until the stress σ_{33} approaches zero. For each iteration the stress is evaluated by the interaction forces acting between pebbles [7]. The assemblies generated by means of the RCP contain 5000 mono-sized ellipsoidal particles of Li_4SiO_4 packed in a virtual cubic box. Simulations with a starting PF ranging from $\sim 62.5\%$ to $\sim 64.27\%$ were carried out to study its impact on the assemblies' mechanical behaviour. The starting packing factors are obtained from the Random Close Packing algorithm described in Section 2.2. The assemblies generated here by this algorithm perfectly resemble the bulk packing structure obtained in packing experiments [14]. This algorithm is suitable to generate densely packed initial structures practically free of overlaps without the use of artificial gravity or preloading. Thus, a low number of contacts occur at the beginning. During the very first few compression steps the number of contacts between particles rapidly increases (see Fig. 9) approaching a strongly reduced rate of growth. However, the variation of the PF during these very first few compression steps is insignificant. Therefore only the initial packing factor obtained from the RCP is reported.

The radius of the primary spheres is set to 0.25 mm. The influence of the particle shape was examined by varying the aspect ratio

Table 1
Physical and mechanical properties of pebbles.

Parameter	Value
Density of bulk material ρ	2260 kg/m ³ [29]
Young's modulus E	90 GPa [30]
Poisson Ratio ν	0.25 [30]
Friction coefficient μ	0.1 [7]
Shear Stiffness k_s	~ 55 GPa

in the range ~ 1.03 –1.12. The investigated range is consistent with the sphericities of the currently produced pebbles. Sphericities of 1.03 and 1.05 are reported in Refs. [4,5], respectively. Aspect ratios higher than 1.05 are representative of fabrication processes resulting in pebbles with a lower sphericity. The authors considered 1.12 the maximum aspect ratio to be appropriately simulated by 3 primary spheres. The reported aspect ratios have been rounded at the second digit. The physical and mechanical properties used are given in Table 1. In this work the shear stiffness is $k_s = 16/3G_{\text{eff}}$ [28], where $G_{\text{eff}} = E/4(1 + \nu)(2 - \nu)$.

4.1. Numerical results

The simulated stress-strain curves of assemblies consisting of ellipsoidal particles with an aspect ratio equal to ~ 1.12 and characterized by different initial PFs are reported in Fig. 7a. In agreement with the previous studies carried on assemblies of spherical pebbles [7] the initial PF was found to noticeably affect the mechanical response of the investigated assemblies. A slight modification of the initial PF results in a considerable variation of the generated stress state, which has potential impact on the overall thermo-mechanical properties of the beds. Reducing the initial PF the assemblies exhibit a more compliant behavior. As will be expected, the residual strain after unloading increases with the reduction of the PF. In particular, the assembly characterized by the highest PF shows the stiffer behavior (higher stress for a given strain) with the lowest residual strain of about 0.8% after the unloading. The generated stress at the end of loading reaches about 3.5 MPa. At the other end, the loosely packed assembly shows (PF = 62.5%) a lower stress build-up for the same maximum imposed strain. This assembly reaches a maximum stress of 0.35 MPa at the end of loading showing a residual strain of 1.16% after unloading. This indicates a massive rearrangement of the elastic particles contained in the assemblies during the compression. Using the in-house DEM code previously developed [15], assemblies of mono-sized spheres with initial PFs similar to those reported in Fig. 7b for assemblies of ellipsoidal particles have been generated and successively investigated. The spheres radius is set to 0.25 mm and the material parameters reported in Table 1 are used. The obtained stress-strain curves are compared with those of ellipsoidal particle assemblies in Fig. 7a.

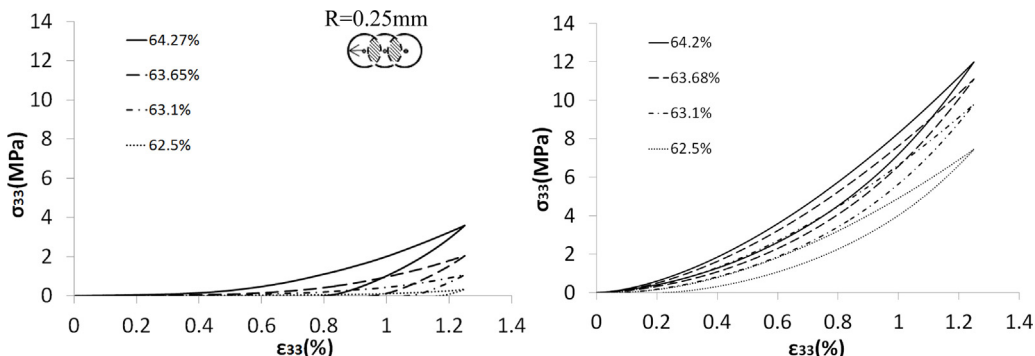


Fig. 7. Stress-strain curves for compressive load concerning assemblies (a) of 5000 ellipsoidal particles with $a_r \sim 1.12$ equal-packed and (b) of 5000 spheres with $R = 0.25$ mm.

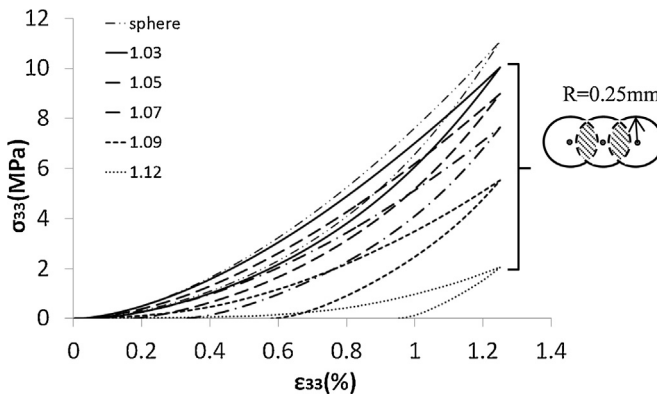


Fig. 8. Stress strain curves for compressive load on assemblies of 5000 ellipsoidal particles, PF $\sim 63.66\%$ with aspect ratios in the range 1, ..., ~ 1.12 .

The assemblies composed of mono-sized spheres show a much stiffer mechanical response than the equivalently packed assemblies of ellipsoids with a relatively small or even negligible residual strain after unloading. This evidences that assemblies of mono sized spheres are more close to their maximum achievable PF in comparison to assemblies of ellipsoids with the same initial PF. Therefore even if the initial packing factor is the same, the assemblies of ellipsoidal particles are less dense in this sense of being more far away from the theoretical maximum PF of $\sim 74\%$ [31]. This suggests that a slight deviation from a perfectly spherical shape can remarkably influence the packing behaviour of a pebble bed, shifting the maximum obtainable PF to higher values. Furthermore, during the compression (or packing) the ellipsoidal particles have a higher mobility in the assembly (in comparison with spherical pebbles) due to the extra degree of freedom associated to the rotation. Particles can change their orientation finding more easily a new equilibrium configuration compared to spherical pebbles. This, together with the assembly being more far away from its maximum PF, explains the softer mechanical behavior of the investigated ellipsoidal assemblies.

Sensitivity studies were performed on assemblies composed of ellipsoidal particles varying the aspect ratio in the range ~ 1.03 – 1.12 . These assemblies have the same initial packing factor of about 63.65–63.66%, the results are reported in Fig. 8. The curves exhibit a strong dependence of the mechanical behavior on the particle shape. A small reduction of the aspect ratio results in a remarkable increment of the maximum stress and in a distinct reduction of the residual strain after unloading. Decreasing the aspect ratio from around 1.12–1.03, the behavior of the investigated assemblies becomes stiffer approaching the curve of the spherical particles of 0.25 mm of radius. This is an evidence of the proper implementation of the method for non-spherical particles presented in this paper. The increase of the maximum stress at the end of loading was found to be nonlinear with the reduction of the particles' aspect ratio. As a consequence of the results reported in Fig. 8, the influence of the particle shape on the pebble packing behavior can be stated such that even if the assemblies are generated with very similar PF, assemblies with higher aspect ratio in the simulated range are more far away from the corresponding maximum obtainable PF.

We attribute the more compliant mechanical behavior of the assemblies consisting of ellipsoidal particles, compared to the equivalent packed assembly of spheres to two reasons. The first one is that structures generated with ellipsoidal particles are more far away from their respective maximum obtainable PF in comparison to assemblies of spheres with same PF, in particular for the assemblies with higher aspect ratio. The second reason is the higher mobility of the ellipsoidal particles, due to additional degrees of

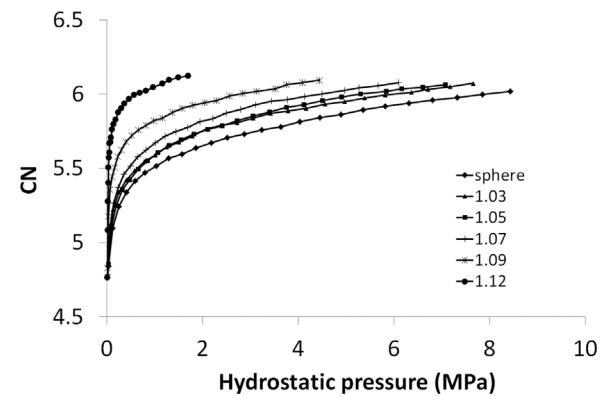


Fig. 9. Coordination number as a function of hydrostatic pressure for assemblies of particles with a PF about of 63.66% and aspect ratios in the range 1, ..., ~ 1.12 .

freedom in rotation, compared to spheres. The slightly different mechanical behavior between spheres and ellipsoidal particles with an aspect ratio of ~ 1.03 is mainly due to the higher mobility of the ellipsoids in the assembly while we associate the softer behavior at higher aspect ratios to these structures being more far away from their maximum PF, mostly.

These statements are further validated by the graphs reported in Figs. 9 and 10. Fig. 9 shows the coordination number (CN) evaluated for the loading path, in function of the hydrostatic pressure. The coordination number is the average number of contacts per particle and calculated as the ratio between the total number of the contacts and number of particles in the assembly. In cases of ellipsoidal particles, eventual multiple contacts between a pair of particles are counted as a single contact. For a fixed value of hydrostatic pressure the coordination number increases with increasing aspect ratio. This confirms that ellipsoidal particles with a higher aspect ratio rearrange more easily with the result of increasing their contacts with the neighbours. As a consequence a higher coordination number is reached at the same level of hydrostatic pressure.

Fig. 10 exemplarily displays the oedometric modulus during the unloading path in function of the uniaxial strain for different aspect ratios. The oedometric modulus (E) was continuously calculated as $E_i = \Delta\sigma_{33,i}/\Delta\epsilon_{33,i}$ during the unloading until the stress in the assembly approaches zero. Here $\Delta\epsilon_{33,i}$ is the difference of the strain between two consecutive time steps while $\Delta\sigma_{33,i}$ is the relative stress change. In order to smooth out numerical oscillations of E_i , the value of the oedometric modulus to be plotted in Fig. 10 at each strain step is obtained by averaging consecutive values of E_i . The calculated values were then reported in Fig. 10 in function of the mean values of the strain evaluated in the corresponding range.

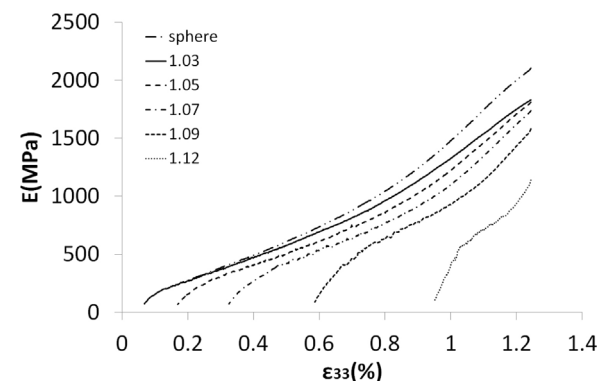


Fig. 10. Oedometric modulus in function of the hydrostatic pressure for assemblies of 5000 particles, PF $\sim 63.66\%$ and aspect ratios in the range 1, ..., ~ 1.12 .

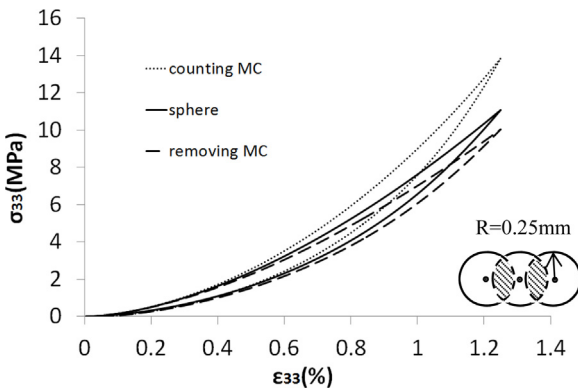


Fig. 11. Comparison between mechanical behavior of equal-packed assemblies (PF $\sim 63.66\%$) of spheres ($R = 0.25\text{ mm}$) and of ellipsoidal particles ($a_r \sim 1.03$) whether counting or not MCs.

A decrease of E with releasing the compressive load is observed for all investigated aspect ratios. For a fixed value of strain the oedometric modulus decreases with increasing the aspect ratio. This confirms that assemblies of ellipsoidal particles have a more compliant mechanical behavior and this effect is enhanced with higher aspect ratio. All these observations together fit into the picture that it is easier to impart deformation in systems of ellipsoidal particles compared to spheres.

The results described above have been obtained by implementing in the code the method described in a previous section to reduce the influence of MCs. For a broader understanding of the issue, the influence of MCs was investigated.

In Fig. 11 three stress–strain curves are reported: the solid line is related to the assembly of spheres with a radius of 0.25 mm, the dotted and the dashed line refer to assemblies of ellipsoidal particles with an aspect ratio of ~ 1.03 accounting for MCs and not, respectively. The initial PF is $\sim 63.66\%$ in all three cases. Accounting for the additional contact forces introduced by the MCs an overestimation of the stress is observed. The simulated curve gets over even the stress–strain curve of the sphere assembly. We judge this as an unrealistic behavior compared to true ellipsoids.

The coordination number, as a function of the strain is reported in Fig. 12. Here, the dotted and the dashed line show the average number of the contacts for a particle accounting for MCs and not, respectively.

The method implemented in the code to reduce the influence of the MCs introduces an asymptotic approximation towards the results of sphere assemblies, as Höhner et al. highlights in Ref. [12]. Moreover, in our work a non-linear contact law was applied, unlike

the linear contact model implemented in Ref. [12], to represent a more realistic contact model. This non-linearity is assumed to lead to an enhancement of the approximation in the results. For this reason further sensitivity studies are required to define the range of applicability of this theory.

5. Conclusions

Nearly spherical pebbles with a small deviation from a perfectly round shape are currently produced by different fabrication processes. In this work, the influence of the particle shape on the mechanical behavior of the whole assembly was investigated numerically. Simulations of axial compression under periodic boundary condition were carried out on assemblies of ellipsoidal particles. Sensitivity studies with different initial packing factors and aspect ratios were performed and the results were compared to those of sphere assemblies in terms of the overall stress–strain curve.

The KIT-DEM code, previously developed for spherical particles, was further extended to study the bulk behavior of assemblies composed of ellipsoidal particles. The original KIT-DEM code was used as reference to demonstrate the consistency of the implemented modifications. Unit quaternions were used to represent the rotational motion of the ellipsoidal particles in the assembly. The ellipsoidal particles are generated by means of the multi sphere method by clustering three primary spheres together. As a consequence the robust contact algorithm developed for spherical particles is still applicable; however multiple contacts between particles may occur. The multi contacts affect the resulting contact forces leading to an overestimation of the generated macroscopic stresses. The methods proposed to reduce the influence of the multi contacts lead to an approximation of the exact solution especially when a non-linear contact law is used.

In agreement with previous studies carried out on assemblies of spherical pebbles, the initial packing factor was found to noticeably affect the mechanical response of the investigated assemblies of ellipsoidal particles. Comparing the results with the mechanical behavior of equally-packed sphere assemblies, more compliant responses were observed in the assemblies of ellipsoidal particles in addition to a relatively high residual strain after unloading. This is an evidence of ellipsoidal particle assemblies being more far away from their theoretical maximum PF in comparison to the sphere assemblies for the same given initial PF. Moreover, the ellipsoidal particles have a higher mobility than spherical pebbles due to the extra degree of freedom associated with the rotation. Particles can change their orientation finding more easily a new equilibrium configuration compared spherical pebbles.

Results of sensitivity studies with different aspect ratios show a remarkable influence of the particles shape on the mechanical response for a given packing factor. A stiffer behavior was observed for assemblies with a lower aspect ratio. In particular, decreasing the aspect ratio, the macroscopic stress–strain curve of an equally-packed sphere assembly was approached, which is evidence of the effectiveness of the implemented modifications, especially with respect to MCs.

In the present work, mono-sized particles with uniform sphericity were simulated. It gives for the first time a basic understanding of the influence of the particle shape on the macroscopic response of breeder pebble beds. Thus, it represents the first step towards the discrete element simulation of pebble beds composed by ellipsoidal particles, which in more general cases may consist of polydispersed beds with particles having a distribution of aspect ratios. The results suggest that pebbles with a poor sphericity cannot be adequately represented by assemblies of perfectly spherical particles. Furthermore, the results will be helpful for both the advancement

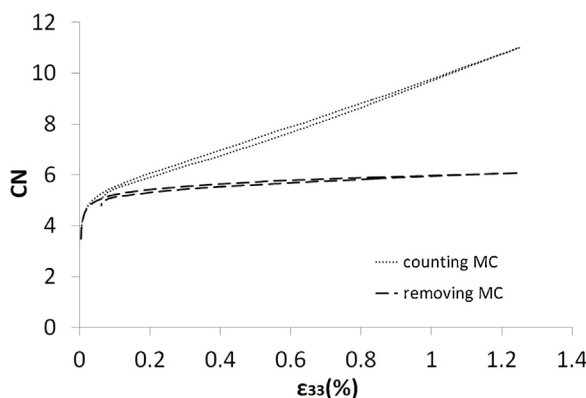


Fig. 12. The evolution of coordination number for given values of strain whether counting or not the MCs.

of breeding zone design and pebble production. However, further investigations are needed to give a more realistic picture of the influence of the pebble shape.

Acknowledgment

This work has been partially supported by the Deutscher Akademischer Austauschdienst–DAAD. The funds were used for a research stay of two months at School of Civil Engineering, The University of Sydney.

References

- [1] T. Shikama, et al., Status of development of functional materials with perspective on beyond-ITER, *Fusion Eng. Des.* 83 (2008) 976–982.
- [2] A. Ying, et al., Status and perspective of the R&D on ceramic breeder materials for testing in ITER, *J. Nucl. Mater.* 367–370 (2007) 1281–1286.
- [3] A. Ying, et al., Status of ceramic breeder pebble bed thermo-mechanics R&D and impact on breeder material mechanical strength, *Fusion Eng. Des.* 87 (2012) 1130–1137.
- [4] T. Hoshino, Development of fabrication technologies for advanced tritium breeder pebbles by the sol-gel method, *Fusion Eng. Des.* 88 (2013) 2264–2267.
- [5] Knitter, et al., Fabrication of modified lithium orthosilicate pebbles by addition of titania, *J. Nucl. Mater.* 442 (1–3) (2013) S420–S424.
- [6] G. Lu, J.R. Third, C.R. Müller, Discrete element models for non-spherical particle systems: fFrom theoretical developments to applications, *Chem. Eng. Sci.* 127 (2015) 425–465.
- [7] Yixiang Gan, Marc Kamlah, Discrete element modelling of pebble beds: with application to uniaxial compression tests of ceramic breeder pebble beds, *J. Mech. Phys. Solids* 58 (2010) 129–144.
- [8] R.K. Annabattula, et al., Mechanics of binary and polydispersed spherical pebble assembly, *Fusion Eng. Des.* 87 (2012) 853–858.
- [9] G. Lu, J.R. Third, C.R. Müller, Critical assessment of two approaches for evaluating contacts between super-quadratic shaped particles in DEM simulations, *Chem. Eng. Sci.* 78 (2012) 226–235.
- [10] D. Markauskas, Discrete element modelling of complex axisymmetrical particle flow, *MECHANIKA* 6 (62) (2006), ISSN 1392–1207.
- [11] D. Markauskas, R. Kačianauskas, A. Džiugys, R. Navakas, Investigation of adequacy of multi-sphere approximation of elliptical particles for DEM simulations, *Granul. Matter* 12 (2010) 107–123.
- [12] D. Höhner, et al., Comparison of the multi-sphere and polyhedral approach to simulate non-spherical particles within the discrete element method: influence on temporal force evolution for multiple contacts, *Powder Technol.* 208 (2011) 643–656.
- [13] W.S. Jodrey, E.M. Tory, Computer simulation of close random packing of equal spheres, *Phys. Rev. A* 32 (4) (1985) 2347–2351.
- [14] Yixiang Gan, Marc Kamlah, Jörg Reimann, Computer simulation of packing structure in pebble beds, *Fusion Eng. Des.* 85 (2010) 1782.
- [15] Yixiang Gan, Thermo-Mechanics of Pebble Beds in Fusion Blankets, 2008, PhD thesis <http://bibliothek.fzk.de/zb/berichte/FZKA7455.pdf>.
- [16] Wolfram Mathematica 13.0, 2015 <http://www.wolfram.com/>.
- [17] K.L. Johnson, *Contact Mechanics*, Cambridge University Press, Cambridge, 1985.
- [18] N. Bicanic, Discrete element methods, in: Erwin Stein, Rene de Borst, Thomas J.R. Hughes (Eds.), *Encyclopedia of Computational Mechanics*, vol. 1, John Wiley and Sons, 2004, pp. 311–337.
- [19] C.A. Truesdell, *A First Course in Rational Continuum Mechanics*. Vol. 1: General Concepts, 2nd ed., Academic Press, 1991, pp. 8–10, III, Sects. I.
- [20] W.C. Swope, et al., A computer simulation method for the calculation of equilibrium constants for the formation of physical clusters of molecules: application to small water clusters, *J. Chem. Phys.* (1982) 76–637.
- [21] L. Verlet, Computer experiments on classical fluids. I. Thermodynamical properties of Lennard-Jones molecules, *Phys. Rev.* 159 (1) (1967) 98–103.
- [22] W.R. Hamilton, On Quaternions, or on a new system of imaginaries in Algebra, *Lond. Edinburgh Dublin, Philos. Mag. J. Sci.* 15–36 (1844) 1–306, 3d Series.
- [23] I. Kosenko, Integration of the equations of a rotational motion of a rigid body in quaternion algebra. The Euler case, *J. Appl. Math. Mech.* 62 (2) (1998) 193–200.
- [24] E. Celledoni, N. Säfström, Efficient time-symmetric simulation of torqued rigid bodies using Jacobi elliptic functions, *J. Phys. A. Math. Gen.* 39 (19) (2006) 5463–5478.
- [25] E. Hairer, G. Vilmart, Preprocessed discrete Moser Veselov algorithm for the full dynamics of a rigid body, *J. Phys. A Math. Gen.* 13 (42) (2006) 13225–13235.
- [26] F. Zhao, B.G.M. vanWachem, A novel Quaternion integration approach for describing the behavior of non-spherical particles, *Acta Mech.* 224 (2013) 3091–3109.
- [27] S.A. Whitmore, L. Hughes, Calif: Closed-Form Integrator for the Quaternion (Euler Angle) Kinematics Equations, US patent (2000).
- [28] S. Zhao, et al., Failure initiation and propagation of Li₄SiO₄ pebbles in fusion blankets, *Fusion Eng. Des.* 88 (2013) 8–16.
- [29] B. Loebbecke, R. Knitter, Procurement and quality control of Li₄SiO₄ pebbles for testing of breeder unit mock-ups, in: Technical Report, Forschungszentrum Karlsruhe, 2007, Fusion Nr. 311, final report on TW6-TTBB-006-D2.
- [30] N. Zaccari, D. Aquaro, Mechanical characterization of Li₂TiO₃ and Li₄SiO₄ pebble beds: experimental determination of the material properties and of the pebble bed effective values, *Fusion Eng. Des.* 82 (15–24) (2007) 2375–2382.
- [31] A. Donev, F.H. Stillinger, P.M. Chaikin, S. Torquato, Unusually dense crystal packings of ellipsoids, *Phys. Rev. Lett.* 92 (2004) 2555061–2555064.